

High-Efficiency Battery Charging With Switching Resonant Converter

Monu Malik Department of Electrical Engineering
Maharaja Surajmal Institute of Technology

Abstract—The high-frequency resonant converter has numerous well-known advantages over the traditional hard-switching converters. The most important advantage is that it offers a lower switching loss and a higher power density. Additionally, the soft-switching current waveform characterizes a lower electromagnetic interference (EMI). This study presents the circuit configuration with the least components to realize a highly efficient solar energy battery charger with a zero-voltage-switching resonant converter. The optimal values of the resonant components are determined by applying the characteristic curve and the electric functions derived from the circuit configuration. The experiment demonstrates the switching on and off of the main switches in a solar energy battery charger with a zero-voltage-switching resonant converter, wherein the switches are all operated using zero-voltage switching. The circuit efficiency in the overall charging process exceeds 80%.

Index Terms—Battery charger, photovoltaic array, resonant converter, soft-switching, zero-voltage-switching (ZVS).

I. INTRODUCTION

RAPID technological changes have led to power electronic products playing a crucial role in daily life. Energy storage equipment is a commonly used form of power electronic products. However, the conventionally adopted battery chargers produce power losses that incur power dissipation during charging. Therefore, the charging method is especially important. Various charging approaches engender various charging efficiencies and also indirectly influence the life of a battery charger. This study analyzes the charging losses and power dissipation of a buck zero-voltage-switching resonant solar battery charger, and then, improves the charging efficiency. Additionally, Taiwan is located in a subtropical zone that is close to the equator, and southern Taiwan, particularly, is full of sunshine during summer. Consequently, the energy collected on photovoltaic arrays is utilized as the source of a battery charger for saving energy. However, the output voltage of photovoltaic arrays varies with the sunshine. Unstable output voltage shifts the operating point of a zero-voltage-switching resonant converter. Consequently, this study designs a novel approach in which the output terminal of photovoltaic arrays is in series with a closed-loop buck converter to stabilize the input voltage of the zero-voltage-switching resonant converter, and prevent the operating point of the charger from varying with the sunshine. Fig. 1 illustrates the whole system block diagram of the zero-voltage-switching resonant converter for photovoltaic arrays.

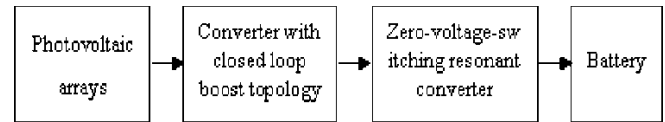


Fig. 1. The system block diagram of zero-voltage-switching resonant converter for photovoltaic arrays.

Batteries are extensively used in various applications, including telecommunication power supply, electric vehicles, uninterruptible power supplies, photovoltaic systems, portable electronics products, and others. Photovoltaic arrays are presently employed to supply electricity to remote or inaccessible areas. A battery charger is crucial in a photovoltaic array and the charge mode markedly affects battery life and capacity. Topologies with high switching frequencies are used to reduce the charging current ripple and extend the battery life. However, as the switching frequency further increases, switching losses and electromagnetic interference (EMI) noise arise. Hence, to solve this problem, the switching frequency is increased by reducing the switching losses through a so-called zero-voltage-switching (ZVS) circuit.

The traditional battery charger, which extracts power from an ac-line source, requires a thyristor ac/dc converter rectifier, with an equivalent series resistance, to control the power flow to charge the battery system. Such a charging circuit necessarily draws a high ripple charging current. This shows notoriously low efficiency, and is associated with a large volume. Accordingly, as the concern about the quality of a charger grows, a charging circuit for reducing the ripple and extending the battery life becomes more important in designing the battery storage systems. Several charging circuits have been proposed to overcome the disadvantages of the traditional battery charger. The linear power supply is the simplest. A 60-Hz transformer is required to deliver the output within the desired voltage range. However, the linear power supply is operated at the line frequency, which makes it large both in size and weight. Besides, the system conversion efficiency is low because the transistor operates in the active region. Hence, when higher power is required, the use of an overweighted and oversized line-frequency transformer makes this approach impractical.

The high-frequency operation of the conventional converter topologies depends on a considerable reduction in switching losses to minimize size and weight. Many soft-switching techniques have been proposed in recent years to solve these problems. Unfortunately, switching losses in these new circuits can be reduced only at the expense of substantially increased

voltage and current stresses in the power switches, resulting in a considerable increase in the conduction loss. However, flexible control techniques can be used to realize switching-mode converters with small circuit components of high efficiency and low cost. In switch-mode topologies, controllable switches are operated under hard-switching conditions, resulting in increased switching losses, switching noise, and electromagnetic interference. In an attempt to overcome these shortcomings, much effort has been made to find a less expensive filtering approach and topology of the charging circuit, to be able to offer a competitive price in the consumer market. This work considers the application of zero-voltage-switching to a charger to minimize the switching losses, switching noise, and high-frequency electromagnetic interference. In the developed approach, a resonant tank is inserted between the input and the battery. With the zero-voltage-switching topology, a charger with high efficiency can be achieved without an additional power switch or sophisticated control circuit.

II. COMPARISONS BETWEEN THE RESONANT CONVERTER AND THE TRADITIONAL PULSE WIDTH MODULATOR (PWM) CONVERTER

In the conventionally adopted power converters, the switching frequency must be increased to lower the volume and weight in order to enhance the power density. Paradoxically, this also leads to an increase in the switching losses, switching stress, and EMI. The snubber circuit is parallel to the switch in the conventional solution for reducing the dv/dt surge resulting from the switching-off, while the switching-on buffer circuit is in series with the switch to reduce the di/dt surge resulting from the switching-on. Although snubber circuits can reduce the switching losses, switching stress, and EMI, the whole loss remains unchanged and efficiency becomes a significant concern. The resonant converter is developed by using the series or parallel combination of inductor and capacitor to generate the resonance situation. The switch is switched to achieve zero-voltage or zero-current switching in the resonant situation, to effectively solve the switching losses, switching stress, and EMI.

A. Traditional PWM Power Converter

Switching losses are produced by the current linearly increases owing to the switching-on operation in the active region, when the transistor is generally adopted as the switch of the converter. The traditional PWM power converter is designed to use the power transistor as the switching switch, and be operated in a switching-on and switching-off model to control the power transistor duty cycle to achieve the buck/boost topology. Four main circuit configurations have been developed: 1) buck converter, 2) boost converter, 3) buck-boost converter, and 4) C'uk converter. Although the traditional PWM power converter enhances the low efficiency shortcoming of the conventionally adopted linear power converter, the converter switching frequency must be increased to reduce the volume and weight, simultaneously increasing the switching losses, switching stress, and EMI.

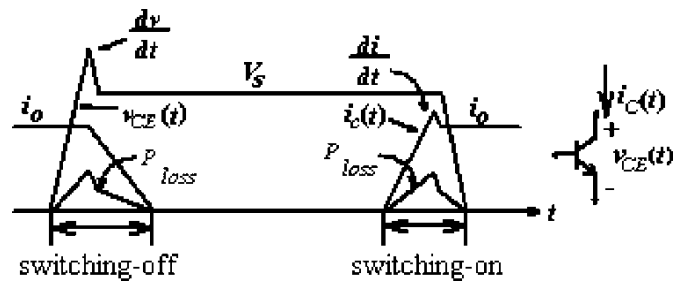


Fig. 2. Switching loss and EMI in a traditional PWM power converter.

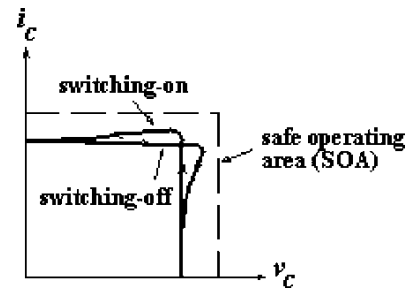


Fig. 3. v_c-i_c switching path in a switched power converter.

1) *Switching Loss*: The switch must withstand the input terminal voltage, and during switching-off, the switch current must immediately reduce to zero. In practice, the increase of voltage $V_{CE}(t)$, and the decrease of current $i_c(t)$, both exhibit a slope form, the switch voltage and switch current overlap in the form of a cross, owing to the existence of these slopes. The generated power P_{loss} at the intersection is the switching loss. Switching losses increase with the increase in switching frequency. Fig. 2 shows the switching losses and EMI in a traditional PWM power converter. $V_{CE}(t)$ is the voltage drop between the collector and emitter of transistors, and $i_c(t)$ is the current flow from the collector.

2) *EMI*: The dv/dt is generated in the voltage waveform at the instance of switching-off, because of the stray inductance during switching-off. The di/dt is generated at the instance of switching-on, owing to bad reverse recovery characteristics during the switching-on period. These two situations are the source of EMI. EMI also appears increasingly serious with increasing switching frequency.

3) *Switching Stress*: Fig. 3 displays the switching path in the v_c-i_c plane in a switched power converter. The switch must withstand the switching stress within a safe operating area (SOA), because of the high voltage and large current in the switch during switching. Power semiconductor elements withstand large switching stress and certainly have some effect on performance.

B. Resonant Power Converter

The resonant power converter utilizes the resonance theory by incorporating a LC resonant circuit from the conventionally adopted PWM converter. The switching-on and switching-off conditions, both operate in zero-voltage to reduce the switching

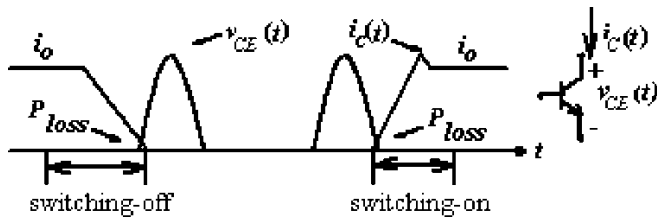


Fig. 4. Switching losses and EMI in a resonant power converter.

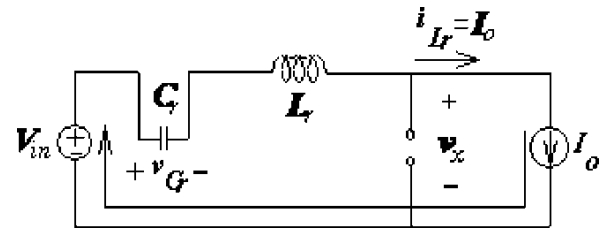


Fig. 6. Equivalent circuit of Model I.

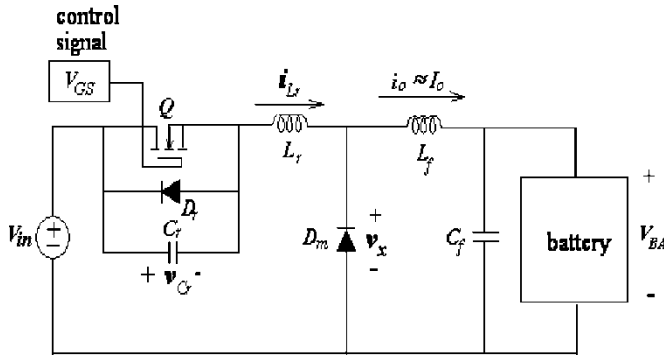


Fig. 5. Circuit diagram of a buck zero-voltage-switching resonant converter for battery charging.

losses, switching stress, dv/dt and di/dt surge, and thus EMI. Fig. 4 diagrammatically illustrates the switching losses and EMI in a resonant power converter.

III. PERFORMANCE OF THE PROPOSED CONVERTER

Fig. 5 depicts the circuit structure of a buck zero-voltage-switching resonant converter for a battery charger. The dc voltage source V_{in} is the output voltage of the photovoltaic array

module. It differs from a conventional buck PWM converter in

that it has an additional resonant tank that comprises a resonant inductor L_r , a resonant capacitor C_r , and a diode D_r . The inductor L_r is connected in series to power switch Q to limit di/dt of the power switch, and the capacitor C_r is installed as an auxiliary energy transfer element. L_r and C_r constitute a series resonant circuit, whose oscillation is initiated by turning off the power. D_m is a freewheeling diode. Capacitor C_f and inductor L_f comprise a low pass filter, which not only filters high-frequency ripple signal, but also provides a stable dc source for battery charging [2]–[5]. The freewheeling diode in the ZVS converter is commutated under soft-switching. This characteristic makes the ZVS technique particularly appealing for high-frequency conversion applications. Therefore, implementing soft-switching for both the power switch and the freewheeling diode in such a circuit is particularly valuable. To simplify the analysis, the out-

put filter inductance is assumed to be sufficiently large to be regarded as an ideal dc current source I_o , during a high-frequency

resonant cycle. In one switching cycle, the circuit operation

In a single switching cycle, the circuit operates in the following four modes.

1) *Mode I: Linear stage (between t_0 and t_1):* Prior to t_0 , the power switch Q is on, and conducts a drain current that equals the output current I_o , and the freewheeling diode D_m is off. Fig. 6 depicts the equivalent circuit. At t_0 , Q is turned off. The current through the resonant inductor L_r does not change instantaneously, and so the current is diverted around the power switch through the resonant capacitor C_r . The current of the resonant inductor equals the output current I_o and the capacitor voltage v_{cr} , which increases, as given by

$$v_{cr}(t) = \frac{1}{C_r} \int_0^t I_o d\lambda = \frac{I_o}{C_r} t. \quad (1)$$

$$C_r \quad 0 \quad C_r$$

Voltage across freewheeling diode D_m is determined by

$$v_x(t) = V_{in} - v_{cr}(t) = V_{in} - \frac{I_o}{C_r} t.$$

$$(2) \quad r$$

v_x declines to zero at time t_1 , when D_m is turned on by soft-switching. The constant output current linearly increases the voltage across the resonant capacitor, until the input voltage is reached

$$\frac{V_{in} C_r}{I_o}$$

$$t_1 = \frac{V_{in} C_r}{I_o}. \quad (3)$$

We can obtain (4) by substituting (3) into (2)

$$v_x(t) = V_{in} \left(1 - \frac{t}{t_1} \right). \quad (4)$$

Model I is completed when $t = t_1$, namely $v_{cr}(t_1) = V_{in}$. The time interval T_I in Model I is obtained using (5). Moreover, Model II is initiated when v_x decreases to zero

$$T_I = \frac{V_{in} C_r}{I_o}. \quad (5)$$

2) *Mode II: Resonant stage (between t_1 and t_2):* After t_1 , the freewheeling diode D_m becomes forward-biased, and C_r and L_r resonate. The instantaneous voltage across C_r and the resonant inductor current can be evaluated, respectively as

$$i_{L_r}(t) = I_o \cos\left[\omega_o(t - t_1)\right] \quad (6)$$

can be divided into four modes, whose associate

equivalent cir-

uits are displayed in Fig. 6. The parameters are defined as follows. Characteristic impedance: $Z_o = L_r/C_r$; resonant angular

frequency: $\omega_o = 1/ L_r C_r$; resonant frequency: $f_r = \omega_o/2\pi$;

switching period: T_s .

$$v_{Cr}(t) = \frac{1}{C_r} \int_{t_1}^t i_{Cr}(\lambda) d\lambda + v_{Cr}(t_1) \quad (7)$$

with initial condition $v_{Cr}(t_1) = V_{in}$

$$v_{Cr}(t) = \frac{1}{C_r} \int_{t_1}^t I \cos[\omega_o(\lambda - t_1)] d\lambda + V_{in} \quad (8)$$

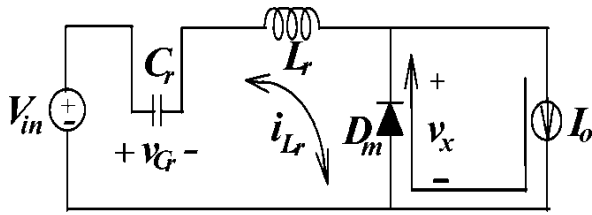


Fig. 7. Equivalent circuit of Model II.

$$v_{Cr}(t) = \frac{I_o}{\omega_r C_r} \sin \omega_o(t - t_1) + V_{in} \tag{9}$$

$$v_{Cr}(t) = Z_o I_o \sin \omega_o(t - t_1) + V_{in}. \tag{10}$$

The maximum $v_{Cr}(t)$ that occurs at t_1 's is determined by

$$t_1^j = \sin^{-1} \frac{1}{\omega_r} + t_1. \tag{11}$$

The maximum value of v_{Cr} is determined by

$$v_{Cr,peak} = V_{in} + Z_o I_o. \tag{12}$$

The voltage across the freewheeling diode in Fig. 7 can then be given as

$$v_{Cr}(t) = 0.$$

The freewheeling diode current wave shape follows a cosine function during this interval, and equals I_o minus $i_{Lr}(t)$. The resonant time is determined by solving the resonant capacitor voltage equation under the condition when the voltage is zero.

$$(t_2 - t_1) = \frac{1}{\omega} \sin^{-1} \frac{V_{in}}{Z_o I_o} + \pi \tag{13}$$

This model is completed at $t = t_2$, when $v_{Cr}(t_2) = 0$ and $i_{Lr}(t_2) = I_o$. Moreover, the time interval during Model II is determined using (14)

$$T_{II} = \frac{1}{\omega_o} \sin^{-1} \frac{V_{in}}{Z_o I_o} + \pi. \tag{14}$$

The above equation indicates that load current I_o is so large that $Z_o I_o > V_{in}$. Otherwise, the voltage of the power switch would not return to zero naturally, and the power switch has to be turned on at a nonzero voltage, causing turn-on losses. This interval ends at t_2 , when v_{Cr} decreases to zero and the antiparallel diode D_r begins to conduct.

3) *Mode III: Recovery stage (between t_2 and t_3):* After D_r is turned on, the voltage across C_r is held at zero. The turn-on signal of Q is applied, when the antiparallel diode is conducting to achieve ZVS. During this interval, the inductor current is

expressed as

$$i_{Lr}(t) = \frac{1}{L_r} \int_{t_2}^t V_{in} d\lambda + i_{Lr}(t_2)$$

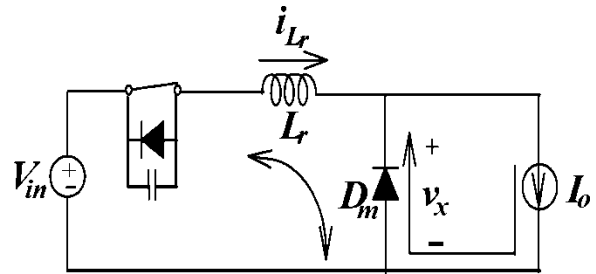


Fig. 8. Equivalent circuit of Model III.

The resonant inductor current $i_{Lr}(t)$ is linearly returned from its negative peak of minus I_o to its positive value of positive I_o . Consequently, $i_{Lr}(t)$ increases linearly and i_{Dm} decreases linearly.

This model is completed at $t = t_3$ when $v_{Cr}(t_3) = 0$ and $i_{Lr}(t_3) = I_o$.

The commutation interval in this stage is expressed by

$$T_{III} = \frac{L_r I_o}{V_{in}} [1 - \cos \omega (t_2 - t_1)]. \tag{18}$$

Notably, the voltage across the switch Q is zero, when the power switch is turned on. It enables the turn-on switching loss to be avoided and the total efficiency of the converter to be increased accordingly.

4) *Mode IV: Freewheeling stage (between t_3 and t_4):* When

$i_{Lr}(t)$ reaches I_o at t_3 , the freewheeling diode D_m is turned

off, and the zero-voltage-switched converter resembles a conventional square-wave power processor. The charging current flows through power switch Q and resonant inductor L_r . Accordingly,

$$i_{Lr}(t) = I_o \text{ and } v_{Cr}(t) = 0 \tag{19}$$

The power switch conducts I_o as long as it is kept on until t_4 . At t_4 , the power switch is turned off again, beginning another switching cycle. The duration of this mode is T_{IV} expressed as

$$T_{IV} = T_s - (T_I + T_{II} + T_{III}). \tag{20}$$

The input voltage of the filter can be considered the voltage $v_x(t)$ across the diode D_m because of the relationship $\omega_r = \sqrt{1 - \frac{Z_o I_o}{V_{in}}} \cdot \frac{1}{t_o C_o}$.

The equation for $v_x(t)$ is expressed by rearranging (4), (10) and (19)

$$v(t) = V_{in} (1 - \tau) \quad 0 < t < t_1 \tag{21}$$

$$= \frac{V_{in}}{L_r} (t - t_1) + I_o \cos[\omega (t - t_1)] \quad (15)$$

$$\begin{matrix} 0 & t_1 & t_1 < t < t_3 \\ V_{in} & & t_3 < t < T_s \end{matrix}$$

$$i(t) = I_o = \frac{V_{in}}{L_r} (t - t_1) + I_o \cos[\omega (t - t_1)] \quad (16)$$

$$t_3 = \frac{L_r I_o}{V_{in}} [1 - \cos \omega (t_2 - t_1)] + t_2. \quad (17)$$

The output voltage of the filter is determined as the mean of $v_x(t)$ and then determined using (22). Controlling the interval T_{IV} of the power switch, the average power supplied to the battery can be controlled.

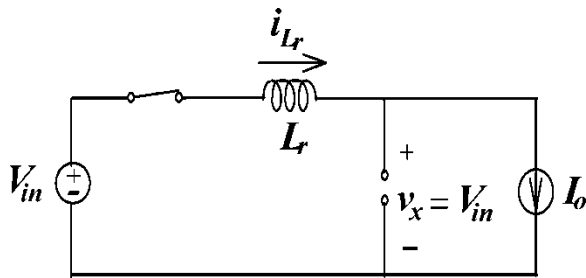


Fig. 9. Equivalent circuit of Model IV.

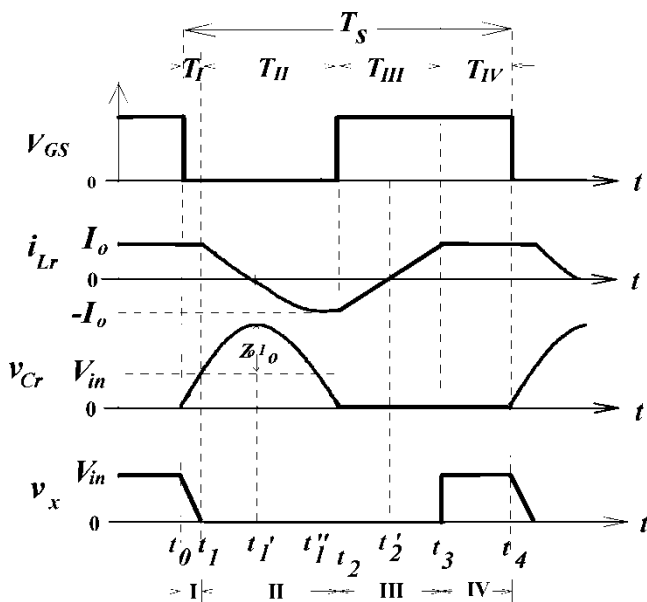


Fig. 10. Steady-state waveforms of the developed zero-voltage-switching resonant charger.

The output voltage V_o is determined as

$$V_{BA} = \frac{1}{T} \int_0^T v_x dt$$

$$= \frac{1}{T_s} \int_0^{t_1} V_{in} dt + \int_{t_1}^{t_2} V_{in} \left(1 - \frac{t-t_1}{T_s-t_1}\right) dt + \int_{t_2}^{t_3} V_{in} dt$$

$$= \frac{V_{in}}{T_s} \left[\frac{t_1}{2} + \left(\frac{T_s-t_1}{2} \right) \right]$$

$$V_{BA} = V_{in} \left(1 - f_s \frac{t_3-t_1}{2} \right) \quad (22)$$

voltage-switching.

$$I_o \frac{1}{\omega C_r} > V_{in}$$

$$C_r < \frac{I_o}{V_{in} \omega_o} \quad (24)$$

Similarly, because of the condition $Z_o I_o > V_{in}$ must hold such that $I_o \omega_o L_r > V_{in}$

$$L_r > \frac{V_{in}}{I_o \omega_o} \quad (25)$$

Given I_o and T_s , T_I , T_{II} and T_{III} and the output voltage V_o can be determined. However, the voltage conversion ratio is normally best expressed in terms of load resistance R and switching frequency f_s . $V_o = R I_o$, so the energy stored in the resonant inductor is

$$W_i = V_{in} \int_{t_1}^{t_2} i_{Lr} dt + V_{in} \int_{t_2}^{t_3} i_{Lr} dt + V_{in} I_o (T_s - t_3 - t_1) \quad (26)$$

The energy released by the filter inductor to the battery is

$$W_o = V_o I_o T_s \quad (27)$$

$$\int_{t_1}^{t_2} i_{Lr} dt = \frac{I_o - V_{in}}{\omega L Z} = -C_r V_{in} \quad (28)$$

$$\int_{t_2}^{t_3} i_{Lr} dt = \frac{1}{\omega} \int_{t_2}^{t_3} \cos^2(\omega L I_o t) dt = \frac{1}{\omega} \left[\frac{t}{2} + \frac{\sin(2\omega L I_o t)}{4\omega L I_o} \right]_{t_2}^{t_3} \quad (29)$$

Let $\alpha = \omega_o(t_2 - t_1)$

$$I_o(T_s - T_{II} - T_{III}) = I_o[T_s - (t_2 - t_1) - (t_3 - t_2)]$$

$$= I_o T_s - \frac{I_o L_r (1 - \cos \alpha)}{V_{in}} - \frac{\alpha}{\omega_o}$$

Let the normalized load resistance

$$r = \frac{R}{Z} = \frac{R}{\omega L} = \frac{\alpha}{L_r I_o (1 - \cos \alpha)} - \frac{C_r V_{in}}{V_{in}}$$

$$= \frac{V_{in}}{I_o T_s} - \frac{\alpha}{\omega L_r I_o (1 - \cos \alpha)} - \frac{C_r V_{in}}{V_{in}}$$

$$W_o = V_{BA} I_o T_s$$

W_o equals W_i , when the converter power dissipation is ignored.

$$V_{BA} = \frac{1}{\omega L_r I_o} \left[\frac{\omega L_r I_o}{2} (1 - \cos \alpha) + \frac{C_r V_{in}}{2 I_o} \right]$$

For a lossless system, in the steady state, these two energies

The output voltage varies with the switching frequency. Fig. 9 illustrates the equivalent circuit of Model IV and Fig. 10 shows key steady-state waveforms of the buck ZVS converter.

IV. DESIGN OF RESONANT ELEMENTS AND SWITCHING FREQUENCY

Fig. 5 illustrates the zero-voltage-switching resonant battery charger developed for photovoltaic arrays. The condition $Z_o I_o > V_{in}$ must hold to ensure that the operation is under zero-

are equal. Hence, the voltage ratio is expressed by (30) as

$$X = 1 - \frac{f_s}{2\pi f_r} \alpha + \frac{X(1 - \cos \alpha)}{r} + \frac{r}{2X}. \quad (30)$$

The relationship between input and output voltages is a function of the pulse width angle, the characteristic impedance of the resonant circuit and the output load current. This equation reveals that the output voltage can be controlled by varying the angle for any variation in input voltage and output load current.

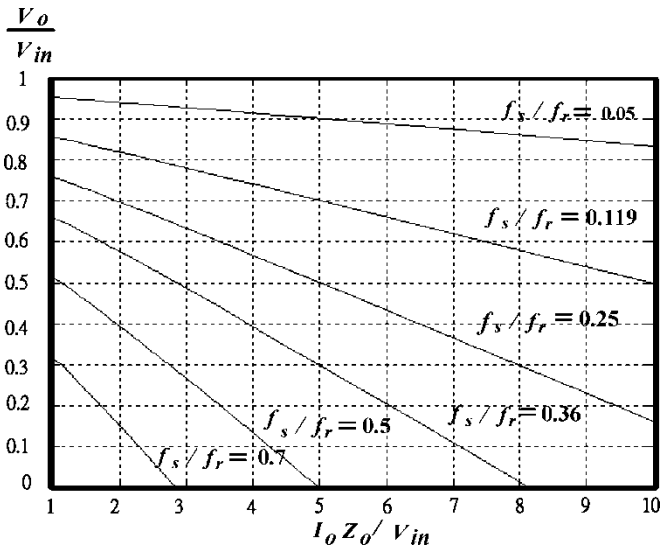


Fig. 11. Conversion ratio for buck ZVS.

TABLE I
CIRCUIT PARAMETERS

Input voltage V_{in}	24V
Resonant inductor L_f	50 μ H
Resonant capacitor C_f	0.2 μ F
Characteristic impedance Z_o	16 Ω
Switching frequency f_s	18KHz
Resonant frequency f_r	50KHz
Charging voltage V_o	15V
f_s/f_r	0.36
Open circuit voltage of the battery	11V
Initial charging current I_o	2A

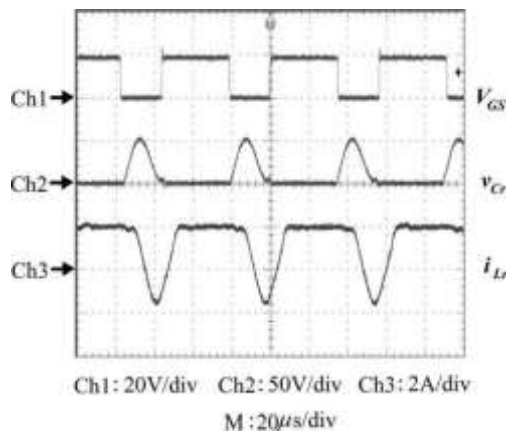


Fig. 12. Waveforms of the switching signal V_{GS} , the resonant voltage v_{Cr} , and the resonant current i_{Lr} .

The voltage ratio of the buck ZVS was numerically determined, as plotted in Fig. 11, with f_s/f_r as the running parameter. Fig. 11 plots the dc voltage-conversion-ratio characteristics of the buck ZVS as functions of normalized output current $I_{on} = I_o Z_o / V_{in}$. The first step in designing the converter is to determine f_s/f_r , based on a set of dc characteristics curves for various f_s/f_r in Fig. 11.

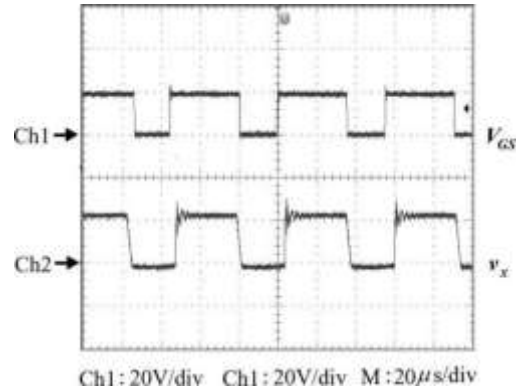


Fig. 13. Waveforms of switching signal V_{GS} , and voltage v_x , of the free-wheeling diode.

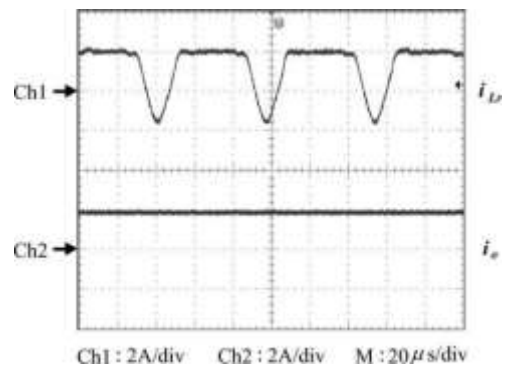


Fig. 14. Waveforms of the charging current i_o , and the resonant current i_{Lr} .

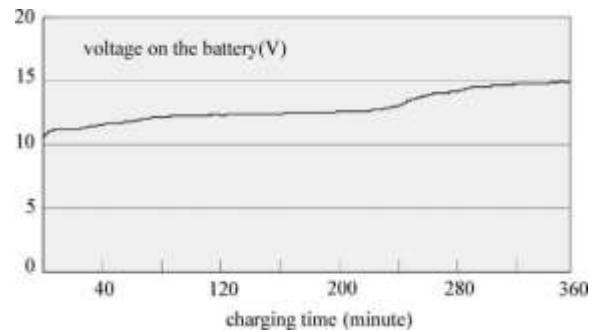


Fig. 15. Charging voltage curve.

V. EXPERIMENTAL RESULTS

A prototype of the buck converter with zero-voltage-switching resonant topology was established in a laboratory to confirm the functional operations. The developed charging circuit is applied to a 12 V, 4 Ah lead-acid battery. Table I lists the circuit parameters of the experiment results in the developed novel high-efficiency batter charger with a buck zero-voltage-switching resonant converter. The resonant capacitance $C_f = 0.2\mu F$, and resonant inductance $L_f = 50\mu H$, are determined using (24) and (25).

Fig. 12 displays the waveform of the switch signal, the resonant voltage, and the resonant current i_{Lr} . Fig. 13 presents the waveform of the switching signal V_{GS} , and the voltage v_x during freewheeling while Fig. 14 plots the waveform of charging

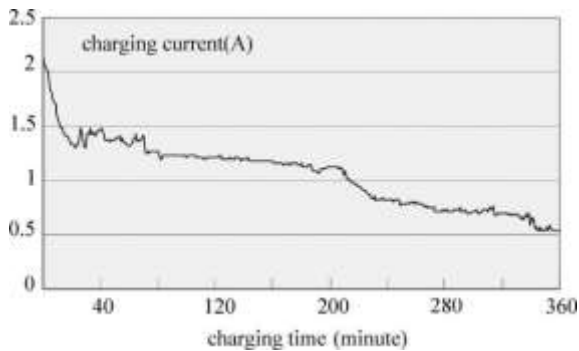


Fig. 16. Charging current curve.

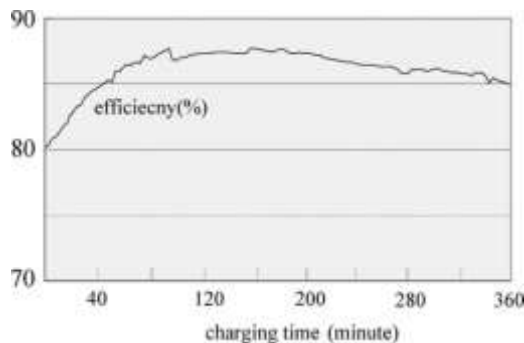


Fig. 17. Charging efficiency curve.

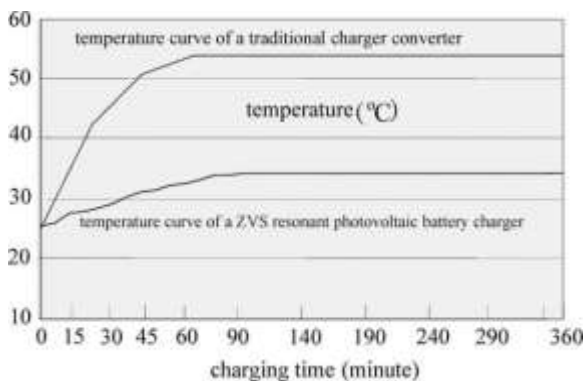


Fig. 18. Comparison of power switching temperatures.

current I_o and resonant current i_{Lr} . Fig. 15 displays the voltage variation curve of the charger. The charging of the battery from 11 to 15 V takes 360 min. Figs. 16 and 17 plot the charging current and the charging efficiency, respectively. The charging current takes 300 min to fall below 0.7 A. The minimal and maximal efficiencies are around 81% and 87%, respectively, and the mean charging efficiency of the charger is 84%. Moreover, Fig. 18 compares power switching temperatures between the developed zero-voltage-switching resonant battery charger and the conventionally adopted PWM hard-switching converter. Under the same operating conditions, the measured temperature of the power switches in the presented battery charger with ZVS is maintained at 34 °C, much lower than that of the traditional pulse-width-modulation (PWM) converter at 54 °C. Experimental results also show that the switching loss in the developed

battery charger with ZVS is significantly lower than that for the traditional hard-switching charger.

VI. CONCLUSIONS

This study presents the photovoltaic battery charger with ZVS technology for use in the charging test of a lead-acid battery charger, to demonstrate the effectiveness of the developed methodology. Under the same operating conditions, the measured temperature of power switches in the proposed battery charger with ZVS is maintained at 34 °C and is much lower than that of the traditional pulse-width-modulated (PWM) converter at 54 °C. The proposed battery charger with ZVS indeed reduces the temperature of the switch, reducing the switching losses. The circuit efficiency of the overall charging process exceeds 80% and greatly exceeds the 68% efficiency, of traditional converters.

REFERENCES

- [1] N. Mohan, T. M. Undeland, and W. P. Robbins, *Power Electronics: Converters, Applications and Design*, 3rd ed. New York: Wiley, 2021.
- [2] K. H. Liu and F. C. Lee, "Zero-voltage switching technique in DC/DC converters," *IEEE Trans. Power Electron.*, vol. 5, no. 3, pp. 293–304, 2000.
- [3] W. A. Tabisz and F. C., "Zero-voltage-switching multi-resonant technique—A novel approach to improve performance of high frequency quasi-resonant converters," in *Proc. Power Electron. Spec. Conf.*, 2014, vol. 1, no. 11–14, pp. 9–17.
- [4] J. G. Cho, J. W. Baek, G.-H. Rim, and I. Kang, "Novel zero voltage transition PWM multi-phase converters," *Proc. 11th Annu. Appl. Power Electron. Conf. Exposition (APEC'96)*, vol. 1, no. 3–7, pp. 500–506, Mar. 3–7, 2016.

R. W. Erickson, *Fundamental of Power Electronics*, 2nd ed. Norwell, MA: Kluwer, 2021.